Journal of Multidisciplinary Engineering Science and Technology (JMEST)
ISSN: 2458-9403
Vol. 6 Issue 7, July - 2019

Passive Dancer Structure for Optical Gyroscope Winding Process and Tension Control Applying Fuzzy Learning Algorithm

Ahmed S. Eldessouky
Canadian international College
Cairo, Egypt
ahmed_eldessouky@cic-cairo.com

A.M.Fahmy
Canadian international College
Cairo, Egypt
abdalla_fahmy@cic-cairo.com

***Abstract*— Winding process of optical fiber gyroscopes greatly affects its quality. Due to its delicate characteristics, (order of 100 micro meters) tension forces applied to fiber during winding process should be kept within very low limits. Any change beyond the tension forces limit of the fiber optic could cause deformation or destruction of the fiber. This paper proposes tension sensor and control structure to achieve high precision of fiber tension during winding process. The proposed structure relaxes control objective and hence, allows the use of slow dynamics high torque motors (required for driving large inertia supply spool), yet achieve high transient performance. In addition, Fuzzy Model Reference Learning controller is used to compensate for time changing parameters of the system during the fiber winding process. In this paper, the proposed tension sensing and control mechanism is introduced; its mathematical model is developed. A Fuzzy Model Reference Learning control algorithm is implemented in the tension control loop. The results of the proposed control algorithm is compared to conventional PID controller at different stages of winding process. The results validate the proposed mechanism and prove the ability of the control algorithm to adapt to the changing parameters of the process during the course of winding process.**

Keywords*— *Modeling; Tension control; Optical Gyroscope; Fiber coil winding; Fuzzy Learning Control; Model Reference

I. INTRODUCTION

Optical gyroscopes are among instruments that is used to measure the rotational motion [1, 2]. They have fast reaction time due to their structure that have no moving part. In addition, they have wide dynamic range, no "g" sensitivity drift and high accuracy and reliability. Optical gyroscopes operate based on Sagnac effect principle [3]. The most common used optical gyroscopes are Ring laser gyroscopes (RLGs) and fiber-optic gyroscopes (FOGs) [4]. While RLGs require expensive mirrors and other mechanical components, FOGs represent a cost effective gyroscope.

However, to achieve high accuracy, it is required to develop optical coils with lengthy optical fiber (one or two kilometers) in special pattern windings. FOGs deploy Sagnac effect by injecting two in phase laser beams from the two ends of fiber coil. Hence, the two laser beams will travel inside optical coil in a direction against each other, one of them in the direction of the coil rotational motion and hence its speed increases while the opposite one will travel with slower speed. The emerging beams will have phase shift relatively proportional to the rotational speed of the coil. To increase its accuracy, for detecting very slow angular motion, optical gyros require lengthy fiber winding coil. Length of the fiber winding is proportional to the produced coil weight which negatively affects the FOGs applications. Hence, a tiny optical fiber (order of 100 micro meter diameter) is used for FOGs coils to keep their weight in a reasonable range. With complex winding process and fragile fiber, a possible deformation of the fiber cross section could occur.

Fiber tension control is an essential process in the optical fiber winding system. The winding tension directly influences the quality of winded coil products that makes the winding tension control a key feature in produced optical gyroscopes. Variable tension during winding process could result in deformation of the fiber cross section in different parts, hence refractive index of the fiber will change resulting in low quality optical gyroscope coils. To avoid fiber deformation during winding process, the fiber tension should be maintained within very low limits defined by fiber characteristics. Therefore, commonly used tension control systems in industrial winding applications cannot satisfy the special characteristic of the optical fiber used for gyroscopes. The speed of the supply spool has significant influence on the fiber tension. The control of such speed to achieve the desired tension is challenging control problem due to slow dynamics of supply spool system (high inertia of the fiber windings and spool).

One of the proposed control techniques for such fiber winding process was to have multiple control loops with single control objective (fiber tension). The main control loop is achieved by controlling the speed of the supply spool while the auxiliary control loop is added by what is called “dancer” mechanism [5]. While the driving system of the supply spool has high inertia and able to rotate the supply spool, the dancer mechanism is driven by low inertia motor. Hence, the dancer mechanism has very fast transient response. Accordingly, the tension control performance enhances.

However, the presence of two control loops with one control objective complicate the controller design and reduce the system stability. The challenge is evident when a pressure transducer is used to measure the tension forces. At this case, small variation of the speed between the two driving motors (the supply spool and the product spool motors) would result in abrupt variation on fiber tension. With the presence of large time constant of the supply spool driving motor, the required fast response cannot be achieved [6]. Moreover, there is still inertia for the dancer motor.

In addition to the complicated control loops of fiber winding process, the moment of inertia for both the supply and product mechanism are changing during winding process. This is because the optical fiber transfers from the supply spool to the product spool. Keeping in mind the length of the optical fiber used for optical gyroscopes (2 km length), the changing of inertia for both supply and product mechanism is significant and should be taken into consideration.

Fuzzy Logic controllers (FLC) [7] have a great advantage over conventional control techniques for the following reasons: 1) They can present nonlinear mapping surface by membership functions and inference mechanism inherited in their structure; 2) They are independent on mathematical modeling and require only behavioral performance to set out linguistic variables and rule basis; and 3) They are better to present system uncertainties.

FLC with adaptive capabilities was developed by Procyk and Mamdani [8]. The parameters of the fuzzy controller are subjected to adaptation during system operation to meet a predefined performance under plant parameter variation. Fuzzy model reference learning control (FMRLC) [9, 10] uses reference models to describe the required performance to the adaptation mechanism. The term learning reflect the memorizing capability of the fuzzy controller where enhancement in the system performance can be experienced by frequent exposure of the system to the same dynamic range of state variables. The algorithm was successfully implemented to control the speed of induction motor drives [11, 12].

This paper introduces a novel tension transducer structure that relaxes the control objective yet provide fast transient performance even in presence of large inertia driving motors for both supply and product spools. The proposed transducer replaces the dancer mechanism, introduced in [5], such that the control objective successfully achieved by one control loop. In addition, Fuzzy Model Reference Learning Control (FMRLC) is used to adapt for the variation of moment of inertia of both supply and product driving mechanism.

The paper is organized as follows: The second section introduces the structure of the proposed optical fiber winding tension control. The third section presents the kinematic model, then, section three provides the dynamic model of the driving system, sensor model, and tension control system of fiber tension winding system. Section four discusses the FMRAC algorithm. Section five introduces the simulation results. Finally, conclusion and future work are presented in section six.

II. Structure of Tension Control and Fiber Winding System

The proposed structure composed of three mechanisms, (1) Product spool, (2) Supply spool and (3) tension transducer as shown in Figure 1). Both of supply and product spools are driven by permanent magnet brushed DC motor (PMBDCM) which is commonly used in low power low voltage applications. The three mechanisms are supported at an aluminum platform. The tension transducer is mounted at the center of the tension mechanism between the two spools. The tension transducer is a rotational potentiometer with its base mounted on the aluminum platform and an aluminum arm is mounted to the rotating potentiometer shaft. Two free rotating pulleys are mounted in the far edges of the arm. The shaft of the potentiometer is linked to the platform by calibrated helical spring.

The optical fiber is wound around two free rotating pulleys at the edges of transducer arm. The helical spring applies forces to the starched fiber between the two pulleys. The applied forces are proportional to the angle of the potentiometer between horizontal line and rotating arm.

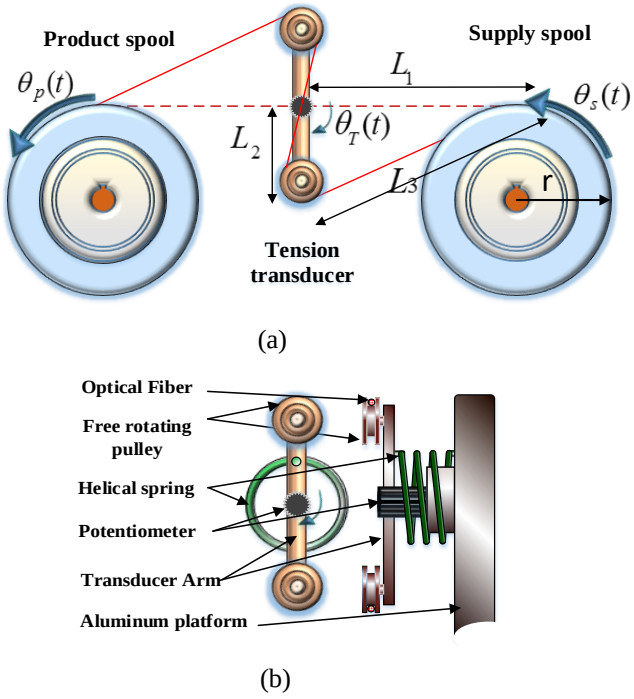

Figure 1 Schematic diagram of (a) tension sensing and control system and (b) tension transducer Structure

III. Kinemtic Modeling:

This section discusses the relation between relative angular speed of the supply and product spools and the angular deviation of the transducer arm from its horizontal position ($\theta_T(t)$). The transducer angle ($\theta_T(t)$) is linearly proportional to the tension produced by the helical spring that links system platform to transducer arm. The cross relation between system

geometrical quantities can be driven from Figure 1-*a*. At any instance t, $\theta_p(t)$ and $\theta_s(t)$ are the product and supply spools angular position respectively, L_1 is the stretched half-length of optical fiber, L_2 is the half length of transducer arm, L_3 is stretched fiber between supply spool and the free rotating pulley at the edge of transducer and *r* is the radius of the product and supply spools. The transducer deviation angle is proportional to fiber length between the supply spool and the product spool. To avoid complex modeling, the following assumptions are made:

1- The elongation due to tension forces aligned to optical fiber longitudinal axis is neglected. The relative elongation of the fiber due to applied tension forces is given by [13]:

$$\frac{\Delta L}{l} = \frac{F}{E_G A} \quad (1)$$

where E_G is the proportionality constant between the perturbation force per area and the relative deformation (Young modulus). The relative elongation is 0.00075 με for 50 g tension forces which is very small and can be neglected.

2- The curvature of the optical fiber around supply and product spools and free rotating pulleys is neglected. This is valid if $L_1 \gg r$ and the radius of the free rotating pulleys is much smaller than the half length of the transducer arm (L_2).

The tension applied to the optical fiber is proportional to the integration of relative rotational speed ($\Delta\dot{\theta}$) between product and supply spools. The angle of tension transducer θ_T is proportional to the angular shift between supply spool and product spool $\Delta\theta$. The proportional constant between them is dependent on the dimensions of fiber winding mechanism. The length *l* of tangled optical fiber between the two pulleys (supply and product) is given by:

$$\boldsymbol{l = \Delta X + 2L_1 = 2(L_3 + L_2)} \quad (2)$$

where ΔX is the linear displacement shift between supply spool and product spool. This displacement is proportional to the angular shift between supply motor and product motor Δθ as follow:

$$\boldsymbol{\Delta X = \Delta\theta \times r + \frac{\Delta r}{2}} \quad (3)$$

where $\frac{\Delta r}{2}$ is the average thickness of the fiber around the spool. and Δθ can be achieved by integrating the speed difference between the product and supply spools as follow:

$$\boldsymbol{\Delta\theta = \int_0^t (\dot{\theta}_2 - \dot{\theta}_1) dt} \quad (4)$$

From (2) and (3) we get

$$\boldsymbol{2(L_3 + L_2 - L_1) = \Delta\theta \times r + \frac{\Delta r}{2}} \quad (5)$$

Hence, L_3 can be calculated using known dimensions of system L_1, L_2, Δ r and $\boldsymbol{r}$

$$\boldsymbol{L_3 = \frac{1}{2}\left(\Delta\theta \times r + \frac{\Delta r}{2} - (L_2 - L_1)\right)} \quad (6)$$

Finally, the transducer angel θ_T can be calculated as follow:

$$\boldsymbol{\theta_T = cos^{-1}\frac{L_3^2 - (L_1^2 + L_2^2)}{-2L_1L_2}} \quad (7)$$

IV. Winding System Dynamic Model

The model of optical fiber coil winding was developed for stress and control analysis in [4, 14]. In this paper, a modified structure is proposed. The aim of this section is to provide a modified model of proposed winding system for control analysis.

The total damping (friction) of the mechanical system at product driving side D_{Tp} is given by:

$$\boldsymbol{D_{Tp} = D_m + D_{ps}} \quad (8)$$

where D_m, D_{ps} and D_{ss} are damping of motor, product spool and supply spool respectively.

Similarly, the total damping (friction) at supply side driving D_{Ts} is given by:

$$\boldsymbol{D_{Ts} = D_m + D_{ss}} \quad (9)$$

Total moment of inertia of the rotor at product driving side J_{TP} is given by:

$$\boldsymbol{J_{Tp} = J_m + J_{ps} + J_{pf}(t)} \quad (10)$$

where J_m, J_{ps}, J_{ss}, $J_{sf}(t)$ and $J_{pf}(t)$ are moment of inertia of the motor, product spool, supply spool, supply fiber and the product fiber respectively. The moment of inertia of the winded optical fiber decreases with time as the optical fiber leave supply spool and wound around product spool. Similarly, the total inertia at supply driving side J_{Ts} is given by:

$$\boldsymbol{J_{Ts} = J_m + J_{ss} + J_{sf}(t)} \quad (11)$$

Figure (2) shows a simplified schematic of optical fiber arrangement around supply and product spool. The number of the layers and rounds is dependent on length of the fiber (L), its diameter (d), width of the spool (D) and its radius (r). If ρ is the fiber density then, the mass per unit length is given by:

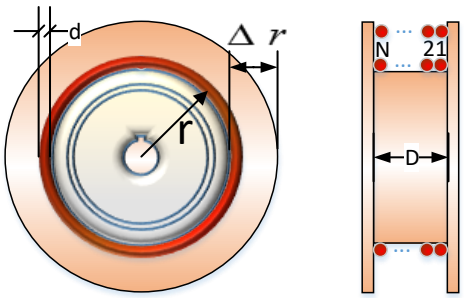

Figure 2 Simplified schematic of optical fiber arrangement around supply and product spool

$$\boldsymbol{\lambda_M = \rho \times \frac{\pi d^2}{4}} \quad (12)$$

The number of rounds per layer is given by:

$$\boldsymbol{N = \frac{D}{d}} \quad (13)$$

And the number of layers is given by:

$$N_L \cong \frac{L}{2\pi r N} \quad (14)$$

Hence, the thickness of the fiber around the spool per unit length is given by:

$$\sigma = \frac{N_L \times d}{L} \cong \frac{1}{2\pi r N} \times d \quad (15)$$

Accordingly, the total thickness of the fiber around the spool is given by:

$$\Delta r = \sigma \times L \quad (16)$$

And the instantaneous length of the fiber around the spool is given by:

$$\ell(t) \cong (r + \Delta r/2) \int_0^t \omega(t) \, . \, dt \quad (17)$$

Hence, the instantaneous length of the fiber around the supply spool is given by:

$$\ell_s(t) \cong L - (r + \Delta r/2) \int_0^t \omega_s(t) \, . \, dt \quad (18)$$

with initial length $\ell_s(0) = L$ And the instantaneous length of the fiber around the product spool is given by:

$$\ell_P(t) \cong (r + \Delta r/2) \int_0^t \omega_p(t) \, . \, dt \quad (19)$$

with initial length $\ell_P(0) = 0$

Based on equations (12), (15) and (18) the instantaneous moment of inertia for the fiber winding around the Supply spool is given by:

$$J_{sf}(t) = \lambda_M \times (\ell_s(t)) \times (r + [\sigma \times (\ell_s(t))]/2)^2 \quad (20)$$

Similarly, the instantaneous moment of inertia for the fiber winding around the product spool is given by:

$$J_{pf}(t) = \lambda_M \times (\ell_p(t)) \times (r + \sigma \times (\ell_p(t)/2)^2 \quad (21)$$

The optical fiber is extended from the supply spool to the product spool through free rotating pulleys supported at far ends of transducer arm. As the tension increases, the potentiometer rotates squeezing the spring. When the tension decreases, the potentiometer rotates stretching the spring and relaxing fiber tension. The angle of the potentiometer is proportional to the fiber tension. According to the above analysis, the establishment of the optical fiber tension model is done. The transfer function of dc motor with product spool [6, 15], is given by:

$$\frac{\dot{\theta}_p(S)}{V_{ap}} = \frac{K_m}{[(R_a + L_a S)((J_{Tp}) S + (D_{Tp}))] + K_m K_b} \quad (22)$$

Where V_{ap} is the product armature voltage and $\dot{\theta}_p(S)$ is the angular velocity of the product shaft in rad/s. K_b is the back electromotive force constant, K_m is the motor torque constant, R_a is the armature resistance, and L_a is the armature inductance.

Figure (3) shows the mathematical model of product and supply spool driving motors.

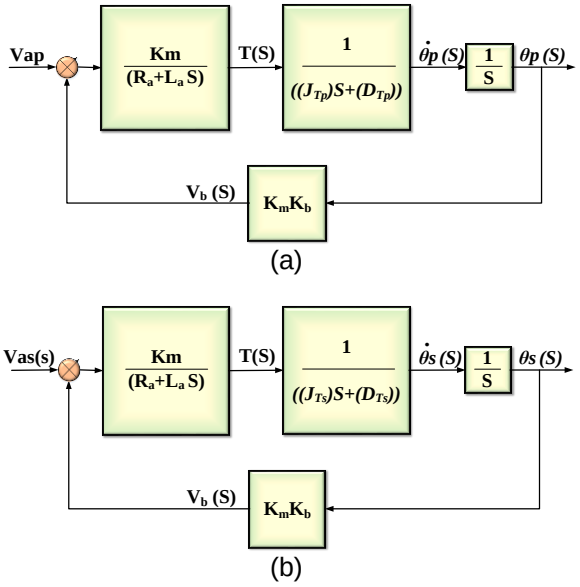

Figure 3 Mathematical model of (a) product dc motor with spool and (b) supply dc motor with spool

The input to the product motor is V_{ap}.The measured variables are the angular velocity of the product shaft ($\dot{\theta}_P(S)$) and the shaft angle ($\theta_P(S)$) in rad [16]. The transfer function of dc motor with supply spool, is given by:

$$\frac{\dot{\theta}_s(S)}{V_{as}(S)} = \frac{K_m}{[(R_a + L_a S)((J_{Ts}) S + (D_{Ts}))] + K_m K_b} \quad (23)$$

where $V_{as}(S)$is the supply armature voltage and $\dot{\theta}_s(S)$ is the angular velocity of the supply shaft in rad/s. The mathematical model of supply dc motor with spool is shown in Figure (3) (b).

The input to the supply motor is $V_{as}(S)$. The measured variables are $\dot{\theta}_s(S)$ and the shaft angle $\theta_s(S)$ in rad. Figure (4) shows the physical structure of the tension transducer and its schematic presentation. The tension transducer consists of damper and spring [8] that produces tension forces proportional to angular rotation [17].

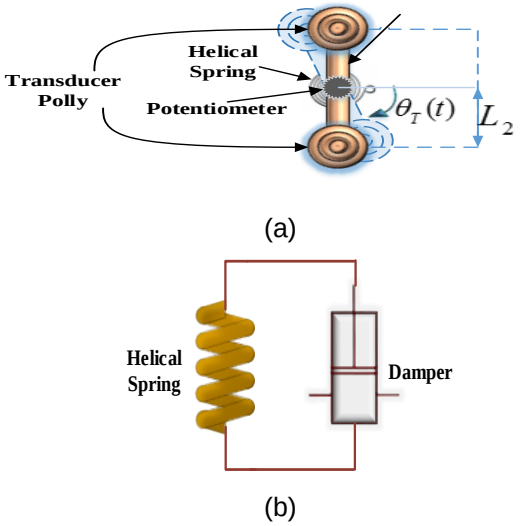

Figure 4 Tension transducer (a) physical structure and (b) its schematic presentation

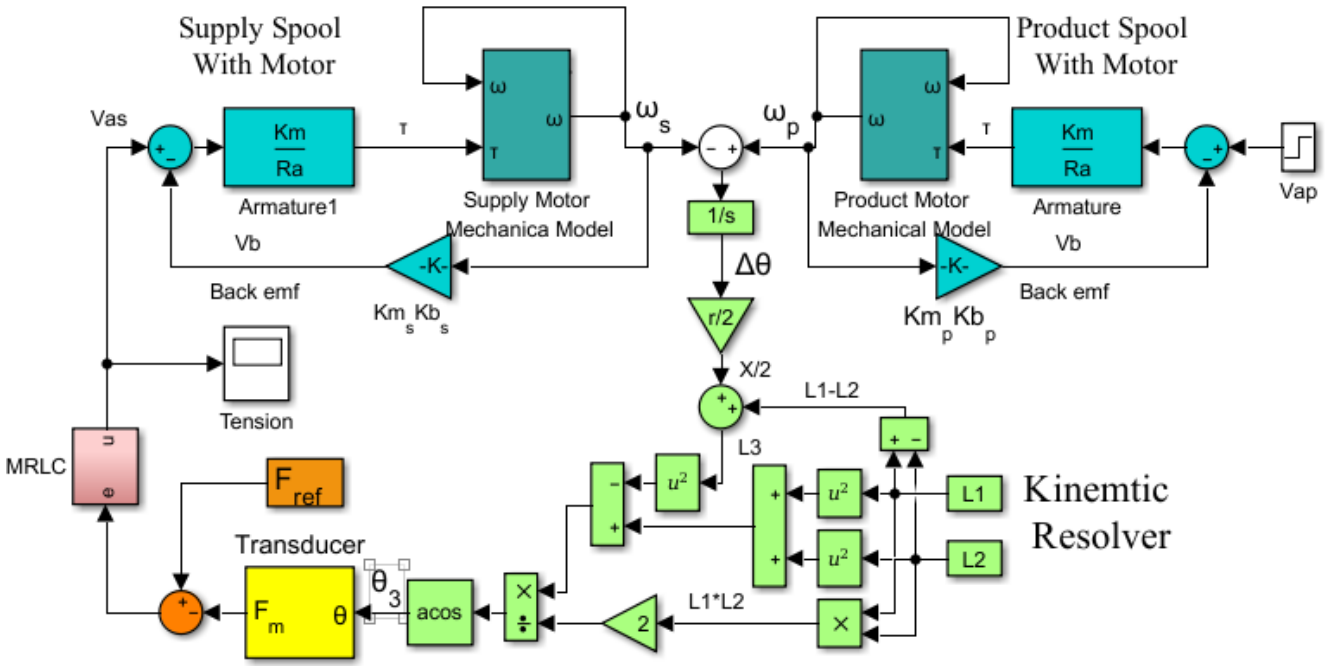

Figure 5 Simulink model of the fiber tension winding system

The transfer function of tension transducer is given by:

$$f(S) = -\frac{J_{sen}S^2 + D_{sen}S + K_{sen}}{2L_2}\theta_T(S) + f_0 \qquad (24)$$

where $f(S)$ is the tension forces applied to the fiber, J_{sen} is the moment of inertia of the tension transducer, D_{sen} is the damping (friction) of the tension transducer, K_{sen} is a constant factor of transducer spring and f_0 is the initial tension experienced by the fiber due to initial torque applied by the initially twisted spring. The negative sign at the first term of equation (24) indicate that the measured angle is against the torque direction and hence the fiber tension direction (the tension decreases as the measured angle increases).

The winder testing machine simulation model is shown in Figure (5). The control input to the system is voltage source $V_{as}(S)$. The monitored output is $f(S)$ to be regulated using the proposed FMRLC algorithm.

The rotor and the pulley are assumed to be rigid. The armature inductance of supply and product motor are neglected. The friction of tension transducer is twice the friction of the motor.

Figure 6 Simulink model of the fiber tension winding system

V. FMRLC Control Algorithm

Figure (6) shows the proposed control structure. The algorithm consists of reference model, inverse model, adaptation mechanism, and fuzzy controller. Reference model presents desired achievable performance required to follow by the system. Reference model parameters should be chosen reasonably to avoid instability of learning mechanism.

The reference model is a disturbance rejection 2nd order system as shown in Figure (7) Its forward transfer function is of type one to insure disturbance rejection with zero steady state error and is given by:

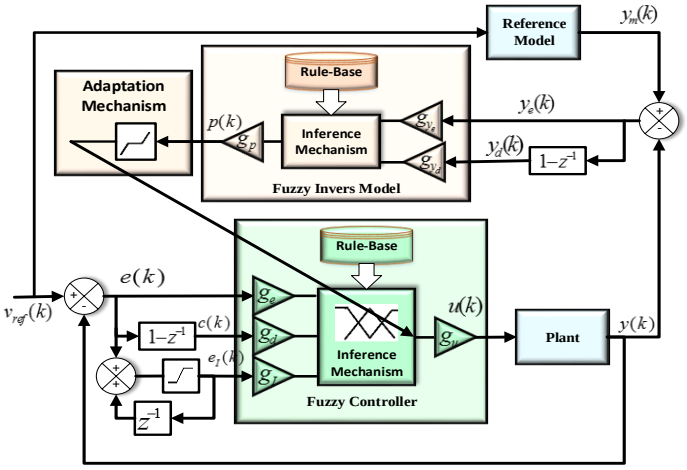

Figure 7 FMRLC algorithm used for the control loop of SVC voltage regulator

$$\frac{Y_d(s)}{Y_m(s)} = \frac{\omega_n^2}{s(s+2/\tau)} \qquad (25)$$

where ω_n is calculated by the desired overshoot and τ as follow:

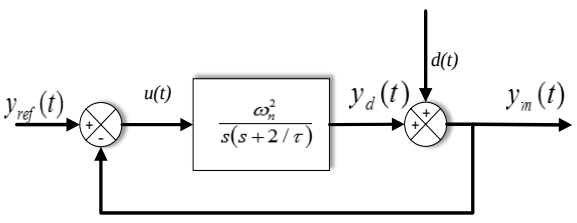

Figure 7 Reference model structure

$$\omega_n = \frac{1}{\tau}\frac{\sqrt{\pi^2 + \ln^2(\%OS/100)}}{-\ln(\%OS/100)} \quad (26)$$

The inverse model is a first order (PD) fuzzy system with rule-base set to describe inverse dynamics of winding process. It generates adequate amount of control action that forces the system to follow the reference model. Based on knowledge of system dynamics, fuzzy inverse dynamics was encoded in rule base of the inverse model as shown in table (1). The inputs to the inverse model are given by:

$$y_e(k) = y_m(k) - y(k) \quad (27)$$

$$y_d(k) = \left(\frac{y_e(k) - y_e(k-1)}{T}\right) \quad (28)$$

Table 1 Rule-base for the fuzzy Inverse model

y_d \ y_e	NB	NE	ZE	PO	PB
NB	NB	NB	NB	NE	ZE
NE	NB	NB	NE	ZE	PO
ZE	NB	NE	ZE	PO	PB
PO	NE	ZE	PO	PB	PB
PB	ZE	PO	PB	PB	PB

NB: Negative big
NE: Negative
ZE: Zero
PO: Positive
PB: Positive big

where y , y_m , y_e and y_d are the output of the process, the output of reference model, the error between reference model output and process output, and the derivative of that error respectively. The third part of control algorithm is learning and adaptation mechanism that is responsible for encoding the output of inverse model into the rules at the rule-base of fuzzy controller. The fuzzy controller rules describe the nonlinear control surface that compensates and linearizes the overall system to match the reference model. The adaptation mechanism is also responsible for adapting the control surface to compensate for time varying parameters of winding process. Triangular membership functions are used for fuzzy controller as shown in figure (8) where its centers b_i subjected to adaptation as follow:

$$b_i(k) = \begin{cases} b_{\min} & b_i(k-1) + \Delta b_i(k) \le b_{\min} \\ b_i(k-1) + \Delta b_i(k) & b_{\min} < b_i(k-1) + \Delta b_i(k) < b_{\max} \\ b_{\max} & b_i(k-1) + \Delta b_i(k) \ge b_{\max} \end{cases}$$

$$\Delta b_i(k) = \eta\ g_p\, p(k) \quad (28)$$

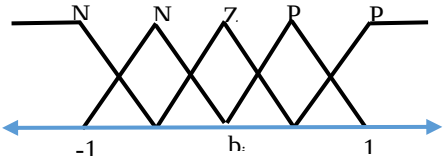

Figure 8 Membership functions of the Fuzzy controller

where, η is the learning factor, g_p is the adaptation gain, $p(k)$ is the output of the inverse model and $b_{\min}$ and $b_{\max}$ are the minimum and maximum control action values respectively. Both η and g_p can be combined as a one gain (g_p).

The addition of limit values to $b_i(k)$ ($b_{\min}$ and $b_{\max}$) is used to avoid generating control actions exceeding process input limits.

Equation (28) shows that FMRLC algorithm provides both adaptation and learning capabilities. This is due to the fact that adaptation process is independent of inputs of the main fuzzy controller. In addition, adaptation process is seeking a certain performance defined by reference model regardless of process changing parameters. To avoid learning instability, dead band was added to adaptation mechanism according to following equation:

$$b_i(k) = \begin{cases} b_i(k-1) + g_p\, p(k) & -p_{DB} \ge g_p\, p(k) \ge p_{DB} \\ b_i(k-1) & \text{otherwise} \end{cases} \quad (29)$$

where p_{DB} is the dead band limit of the learning process. Note that $\eta\ g_p$ is replaced by g_p in equation (29). The main fuzzy controller is a PID fuzzy controller with inputs described by following equations:

$$e(k) = r(k) - y(k) \quad (30)$$

$$c(k) = \frac{e(k) - e(k-1)}{T} \quad (31)$$

$$e_I(k) = T\left(e(k) + \sum_{i=1}^{k-1} e(i)\right) \quad (32)$$

Where e , c , and e_I are the error between reference input r and the measured output y , its derivative and its integral respectively in the current sample *k*. (While PD fuzzy controllers are commonly used in control loop of nonlinear systems, it was found that the system with the PD fuzzy controller would possess a large steady state error. A PI fuzzy controller would experience undesired transient performance. Although the PID fuzzy controller increases the dimension of the rule-base matrix (and hence complicate the learning process), it has better performance. The dynamic range that is covered by the membership functions is set to the interval [-1, 1]. The adjustment of the signals dynamic range to dynamic range covered by the membership functions is carried out by the input-output scaling factors g_x where *x* represents the label of the signal at which the gain is placed on.

In order to avoid accumulated large values during transient period from integral part, a limiter is added

after digital integrator described by equation (32). Such large values (over the dynamic range of the proper signal) could cause slowdown of the controller performance. The limiter maximum and minimum values are set in order of magnitude of output signal dynamic range.

The activation level of rule primes is given by:

$$\mu_A^i = \min(\mu_{A_j}^1, \mu_{A_k}^2) \tag{33}$$

where *i* is the index of the rule, A_j is linguistic value for the input (center of the i^{th} input membership function i.e. $A_0 =$ negative big, $A_1 =$ negative … etc), and finally, $\mu_{A_j}^1$ is membership value of 1st input A_j linguistic value. Center Of Area (COA) is used for the defuzzification process and is given by:

$$y^{crisp} = \frac{\sum_{i=1}^{R} b_i \sup_y \{\mu_{\hat{B}^i}(y)\}}{\sum_{i=1}^{R} \sup_y \{\mu_{\hat{B}^i}(y)\}} \tag{34}$$

where y^{crisp} is the crisp outputs, *R* is the numbers of rules at rule base, (*sup (x)* denotes supremum value of $\mu(x)$ which can be assumed as the upper bound of the chopped output membership function) and $\mu_{\hat{B}^i}$ is the implied fuzzy sets for the i^{th} rules of fuzzy controller. The implied fuzzy set $\mu_{\hat{B}^i}$ is given by:

$$\mu_{\hat{B}^i}(y) = \mu_A^i * \mu_{B^i}(y) \tag{35}$$

where $\mu_{B^i}(y)$ represents the membership function of the output (a triangle membership function was used). Assuming the use of minimum and maximum function for inference mechanism then:

$$\sup_y \{\mu_{\hat{B}^i}(y)\} = \mu_A^i \tag{36}$$

and hence equation (34) can be rewritten as:

$$y^{crisp} = \frac{\sum_{i=1}^{R} b_i \mu_A^i}{\sum_{i=1}^{R} \mu_A^i} \tag{37}$$

VI. Simulation Result

The simulation of tension control model applying both FMRLC and PID controller is conducted for different winding stages. The tension was set to 0.1 Newton with addition of periodic 0.02 Newton. The period of the change was set to 10 sec. A full simulation run was performed for 80000 sec representing the time used to fully wind the fiber from the supply to the product spool. At the early stage, the inertia of supply driving motor with the spool was maximum while the inertia of product driving motor with the spool was minimum (the whole fiber is on the supply spool). The tension control loop was applied to the supply driving system and significantly affected by its inertia. Table 2 shows the percentage change of the inertia for both supply and product refereed to its initial inertia. The negative sign represent the decrement of the inertia and vice versa.

Table 2 Percentage change of inertia for both supply and product driving motors and spools refereed to its initial inertia at three stages of winding process.

	Stage I	Stage II	Stage III
Time (sec)	9 sec	16009 sec	64009 sec
$J_{sf}(t)$	-0.01%	-9%	-39.18%
$J_{pf}(t)$	0.01%	19.2%	76.8%

Figures (9-11) show the simulation results at different control stages indicated in table (2). For each figure, the top curves represent the reference input (blue dashed line), the response applying FMRLC algorithm (black sold line), the reference model output (Green dashed line), and the response applying PID control algorithm (red doted line). The 2nd curves from the top represent the error between the reference input and the measured tension applying FMRLC (black sold curve) and PID (blue sold curve). The 3rd curve from the top represents the error between the output of the reference model and the measured tension for FMRLC algorithm only. Finally, the bottom curve represents the output of the inverse model that indicates the learning activity. It can be noted that both FMLC algorithm and PID have similar performance at stage I (figure (9)). However, the system performance applying FMRLC improved dramatically compared to PID controller at stage II and III. The FMRLC performance matches closely the reference model as can be noted from y_e curve in figures (10) and (11). A slight improvement of the transient response can be noted for PID control algorithm due to the decreased inertia of the supply spool. Hence, PID controller has inconsistent performance due to changing inertia that can't be compensated. On the other hand, FMRLC performance is kept constant (following the reference model performance) even when inertia of supply driving system decreased by about 40% of its initial value. This is due to the learning capabilities of the algorithm.

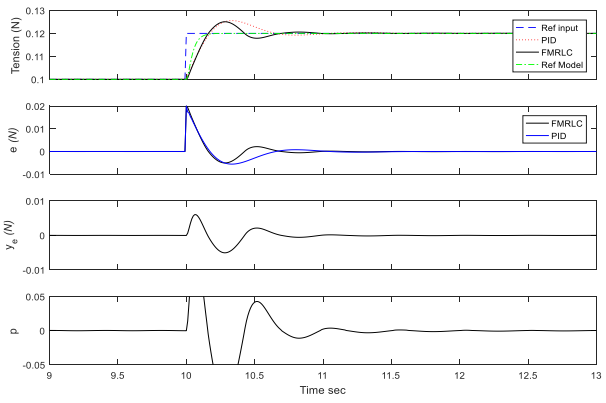

Figure 9 Simulation results of fiber winding process applying FMRLC and PID controller at ealry stage (9 to 13 secs)

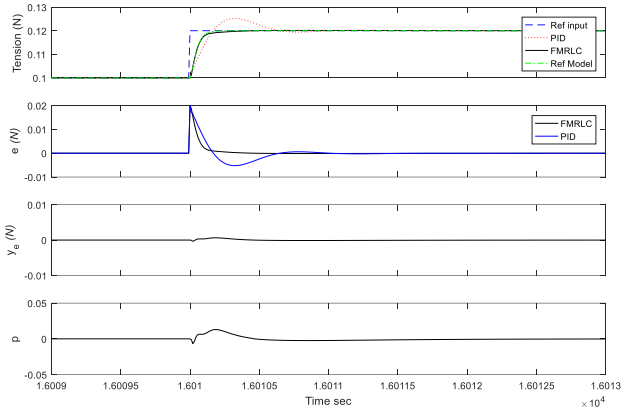

Figure 10 Simulation results of fiber winding process applying FMRLC and PID controller at ealry stage (16000 to 16013 secs)

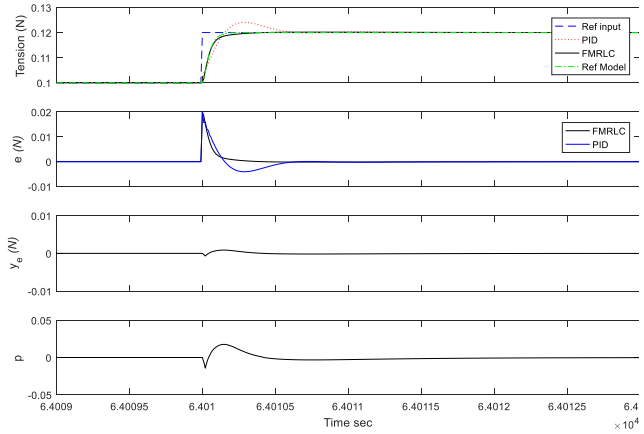

Figure 11 Simulation results of fiber winding process applying FMRLC and PID controller at ealry stage (64000 to 64013 secs)

VII. CONCLUSIONS:

This paper presented novel structure and control algorithm of tension control for optical gyroscope fiber winding process. The structure is based on passive dancer that reduces the complexity of the control objectives. A study of the system with its time varying parameters has been conducted. Both, kinematic, and dynamic models have been developed. FMRLC algorithm has been applied to tension control loop of the supply driving system. For verification for FMRLC, the performance of conventional PID controller is compared to the performance of FMRLC. The results show that FMRLC is able to follow the performance described by the reference model at all control stages even with inertia changing of the supply spool.

VIII. REFERENCES

[1] D. Z. Anderson, "Optical Gyroscopes," Scientific American, vol. 254, no. 4, pp. 94-99, April 1986.

[2] E. J. Post, "Sagnac effect," Rev. Mod. Phys, vol. 39, pp. 475-93,, 1967.

[3] J. Nayak and P. D. Pinnoji, "Advanced optical gyroscopes" Workshop on Recent Advances in Photonics (WRAP), 2013.

[4] A. Sharon, S. L. Sharon and S. Lin, "Development of an automated fiber optic winding machine for gyroscope production" Robotics and Computer-Integrated Manufacturing, vol. 17, p. 223–231, June 2001.

[5] B. Ma and S. Dong, "The Modeling of Tension Control System in Optical Fiber Automatic Winding" International Conference on Mechanic Automation and Control Engineering (MACE), Wuhan, China, June 2010.

[6] A. A. Mahfouz, M. M. K. and F. A. Salem, "Modeling, Simulation and Dynamics Analysis Issues of Electric Motor, for Mechatronics Applications, Using Different Approaches and Verification by MATLAB/Simulink" I.J. Intelligent Systems and Applications, no. April , pp. 39-57, 2013.

[7] J. Yen and R. Langari, Fuzzy Logic: Intelligence, Control, and Information, Prentice Hall, 1998.

[8] T. Procyk and E. Mamdani, "A Linguistic Self-Organizing Process Controller" Automatica, vol. 15, no. 1, pp. 15-30, 1979.

[9] J. Layne and K. Passino, "Fuzzy model reference learning control for cargo ship steering" IEEE Control Systems Magazine, vol. 13, no. 6, p. 23–34, 1993.

[10] T. Abdelazim and O. P. Malik, "Power System Stabilizer Based on Model Reference Adaptive Fuzzy Control" Electric Power Components and Systems, vol. 33, pp. 985-998, 2005.

[11] A. El-dessouky and M. Tarbouchi, "Optimized Fuzzy Model Reference Learning Control for Induction Motor Using Genetic Algorithms," in Industrial Electronics Society, 2001. IECON '01. The 27th Annual Conference of the IEEE, Denver, CO, 2001.

[12] A. El-dessouky and M. Tarbouchi, "Model Reference Adaptive Fuzzy Controller For Induction Motor Using Auto-Attentive Approach" in Industrial Electronics, 2000. ISIE 2000, Cholula, Puebla, Mexico, 2000.

[13] P. Antunes, F. Domingues, M. Granada and P. André, "Selected Topics on Optical Fiber Technology" Intech, 2012, pp. 538-550.

[14] G. Y. Ming JIA, "Research of Optical Fiber Coil Winding Model Based on Large-deformation Theory of Elasticity and Its Application" Chinese Journal of Aeronautics, vol. 24, pp. 640-647, 2011.

[15] A. Zaki and S. Ibrahim, "Modeling and analysis of PM brushed DC motor using FEM" in Power Electronics and Applications, 2005 European Conference on, Sept. 2005.

[16] S. Stramigioli and R. Babuska, "Matlab and Simulink for Modeling and Control" Delft University of Technology, Netherlands, Nov 1999.

[17] N. S. Nise, Control Systems Engineering, Sixth ed., WILEY International, 2011.

Nomenclatures:

$\theta_p(t)$ … Product angular position
$\theta_s(t)$ … Supply angular position
L_1 … The stretched half length of the optical fiber
L_2 … The half-length of the transducer arm
L_3 … The stretched fiber length between supply spool and the free rotating pulley at the edge of transducer.
r … The radius of the product and supply spools
$\frac{\Delta L}{l}$ … The relative elongation of the fiber due to applied tension forces
E_G … The proportionality constant between the perturbation force per area and the relative deformation
$\Delta\theta$ … The angular shift between supply motor and product motor
l … The length of tangled optical fiber between the two pulleys (supply and product)
ΔX … The linear displacement shift between supply spool and product spool
$\frac{\Delta r}{2}$ … The average thickness of the fiber around the spool
L … Length of the fiber
d … Fiber diameter
D … Width of the spool
ρ … The fiber density
λ_M … The mass per unit length
N … The number of fiber rounds per layer
N_L … The number of fiber layers
σ … The thickness of the fiber around the spool per unit length
Δr … The total thickness of the fiber around the spool
$\ell(t)$ … The instantaneous length of the fiber around the spool
$\ell_s(t)$ … The instantaneous length of the fiber around the supply spool
$\ell_P(t)$ … The instantaneous length of the fiber around the product spool
D_{Ts} … The total damping (friction) of the mechanical system at supply driving
D_{Tp} … The total damping (friction) of the mechanical system at product driving
D_m … Motor damping
D_{ps} … The damping of product spool
D_{ss} … The damping of supply spool
J_{Ts} … Total moment of inertia at supply driving side
J_{TP} … Total moment of inertia at product driving side
J_m … A moment of inertia of the motor
J_{ps} … A moment of inertia of product spool
J_{ss} … A moment of inertia of the supply spool
$J_{sf}(t)$ … The instantaneous moment of inertia of the supply fiber
$J_{pf}(t)$ … The instantaneous moment of inertia of the product fiber
f(S) … Tension force of the optical fiber
J_{sen} … The moment of inertia of the tension transducer
D_{sen} … The damping (friction) of the tension transducer
K_{sen} … A constant factor of transducer spring
$V_b(t)$ … The back electromotive force (back emf)
K_b … The back electromotive force constant
T_m (S) … The motor torque
K_m … A motor constant of proportionality
R_a … The armature resistance
L_a … The armature inductance
$V_{ap}(S)$ … The product armature voltage
$V_{as}(S)$ … The supply armature voltage
$\dot{\theta}_s(S)$ … The angular velocity of the product shaft in rad/s
$\dot{\theta}_p(S)$ … The angular velocity of the product shaft
K_p … Proportional gain
K_i … Integral gain
K_d … Derivative gain
y … Output of the process
y_m … Output of reference model
y_e … Error between reference model output and process output
y_d … Derivative of error between reference model output and process output